Hubbard Model on the Pyrochlore Lattice: A 3D Quantum Spin Liquid

B. Normand[1] and Z. Nussinov[2]
[1]Department of Physics, Renmin University of China, Beijing 100872, China
[2]Department of Physics, Washington University, St. Louis, Missouri 63160, USA
(Received 15 September 2013; revised manuscript received 20 December 2013; published 21 May 2014)

We demonstrate that the insulating one-band Hubbard model on the pyrochlore lattice contains, for realistic parameters, an extended quantum spin-liquid phase. This is a three-dimensional spin liquid formed from a highly degenerate manifold of dimer-based states, which is a subset of the classical dimer coverings obeying the ice rules. It possesses spinon excitations, which are both massive and deconfined, and on doping it exhibits spin-charge separation. We discuss the realization of this state in effective $S = 1/2$ pyrochlore materials.

DOI: 10.1103/PhysRevLett.112.207202 PACS numbers: 75.10.Jm, 75.10.Kt, 75.40.Gb

The quantum spin liquid [1] has become the focal point for our understanding of many of the most fundamental issues in strongly correlated systems. These include exotic quantum phases, quantum critical physics, the relevance of broken symmetries, topological order, entanglement, and the possibly fractional nature of elementary excitations in both gapped and gapless states [2]. The search for theoretical realizations of these ideas has led to numerous proposed models, which while highly informative have generally been too simple or abstract to apply to real materials [3]. The search for materials realizations is a very active field where much current attention is focused on kagome systems [4], triangular organics [5], and other frustrated $S = 1/2$ and $S = 1$ quantum magnets. However, materials complexities such as impurities, Dzyaloshinskii-Moriya interactions, spin-orbit coupling, and other anisotropies in real and spin space have to date caused strong departures from theoretical ideals.

Frustrated quantum magnets offer one of the most promising routes to spin-liquid behavior [1,2]. Frustration presents a formidable barricade to theoretical understanding, because the ground manifold is quite generally a set of highly degenerate basis states, with little or no separation emerging in an exact treatment of the interactions [6]. Numerical calculations converge very slowly due to this proliferation of near-ground states [7]. Fluctuations in such a manifold may lead to a range of exotic phenomena [8–10], and the departures mentioned above are strong because any perturbation is strongly relevant in a highly degenerate system. Few exact results are available, although these afford essential insight [11–14].

In this Letter, we discuss the one-band Hubbard model, showing that on a half-filled pyrochlore lattice it gives a highly frustrated intratetrahedral spin model with only weak perturbations. This model contains an exactly solvable Klein point, about which there is an extended region of parameter space where the ground state is a three-dimensional (3D) quantum spin liquid. This state hosts massive spinon excitations, which are deconfined and move in all three dimensions within the lattice. The parameter range for the spin-liquid phase lies exactly in the regime of many magnetic materials.

The pyrochlore lattice, shown in Fig. 1, is a 3D array of corner-sharing tetrahedra, has cubic symmetry, and is a geometry widespread in transition-metal and rare-earth oxides. Most such materials have half-filled bands and are Mott-Hubbard insulators due to their interactions. We begin with the Hubbard model,

$$H_{\rm Hubb} = -t\sum_{\langle ij\rangle,\sigma} c^{\dagger}_{i\sigma}c_{j\sigma} + U\sum_{i} n_{i\uparrow}n_{i\downarrow}, \tag{1}$$

where $c^{\dagger}_{i\sigma}$ creates an electron at site i with spin σ and $n_{i\sigma} = c^{\dagger}_{i\sigma}c_{i\sigma}$ is the number operator. We use it to discuss the spin liquid with no theoretical abstractions and with controlled approximations. A perturbative expansion in t/U for the half-filled band leads to

$$H = H_t + J_3\sum_{\langle\langle ij\rangle\rangle} \vec{S}_i \cdot \vec{S}_j + \mathcal{O}(t^6/U^5), \tag{2}$$

where $\langle\langle ij\rangle\rangle$ denotes next-neighbor site pairs and

$$H_t = \sum_l \left[\frac{1}{2}J_1\mathbf{S}^2_{l,\rm tot} + \frac{1}{4}J_2\mathbf{S}^4_{l,\rm tot}\right] \tag{3}$$

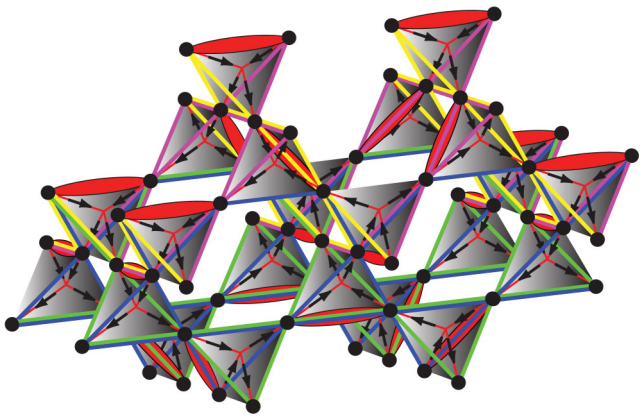

FIG. 1 (color). Pyrochlore lattice. The magnetic ions (black circles) form a 3D array of corner-sharing tetrahedra.

 © 2014 American Physical Society

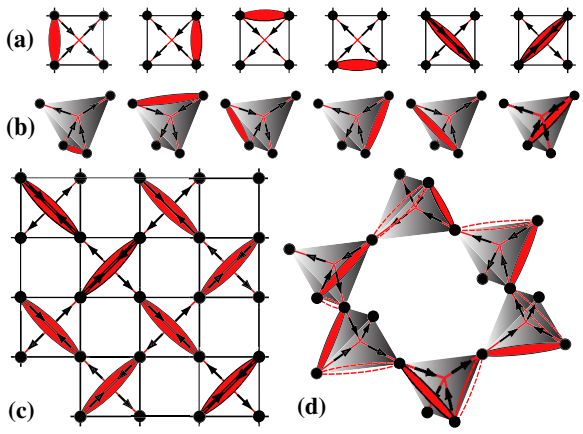

FIG. 2 (color online). One-dimer configurations on a single tetrahedron and their six-vertex representations (a) in 2D and (b) in 3D. (c) The maximally flippable state (all-diagonal dimer covering) of the checkerboard lattice, which requires only two vertex types. (d) One hexagon of the pyrochlore lattice with the dimers of the surrounding tetrahedra in a flippable configuration, as shown by the black arrows; dashed red ellipses indicate the flipped dimer state.

is a sum of purely intratetrahedral spin interactions written in terms of the total spin $\mathbf{S}_{l,\mathrm{tot}} = \mathbf{S}_{l1} + \mathbf{S}_{l2} + \mathbf{S}_{l3} + \mathbf{S}_{l4}$ on each tetrahedron, l [15]. In Eqs. (2) and (3),

$$J_1 = 4t^2/U - 160t^4/U^3 + \mathcal{O}(t^6/U^5),$$
$$J_2 = 40t^4/U^3 + \mathcal{O}(t^6/U^5),$$
$$J_3 = 4t^4/U^3 + \mathcal{O}(t^6/U^5), \quad (4)$$

the very large prefactors in J_1 and J_2 arising from the many permutations of fourth-order processes within the tetrahedron. Thus, $J_3 \ll J_{1,2}$ and to an excellent approximation one has an intratetrahedral Hamiltonian H_t, with only weak interactions coupling spins in different tetrahedra.

H_t (3) has a unique point for one particular parameter ratio $J_2 = J_{2c} = -J_1$, occurring when $t/U = 1/\sqrt{30}$, where all singlet and triplet states of the four spins on each tetrahedron have energy zero (see Supplemental Material [16]). Thus, any tetrahedron containing a dimer, a singlet ($S = 0$) state of any two spins, and represented by red ellipses in Figs. 1 and 2 has energy zero. Furthermore, because the number of dimers equals the number of tetrahedra on the pyrochlore, all states of the whole system with precisely one dimer per tetrahedron (Fig. 1) are exact, zero-energy ground states. The set of classical dimer coverings maps exactly to the six-vertex model, represented by the six possible "two-in, two-out" configurations of the black arrows in Figs. 2(a) and 2(b) and, hence, to the ice problem. Pauling deduced an exponential lower bound on the number of states in this ground manifold $N_g > (3/2)^{N/2}$ with N the system volume (number of tetrahedra) [17], proving that it has extensive degeneracy. This is a Klein point [12,16]. It is a dimer liquid with algebraic correlations, a classical critical point at which all (of the exponentially many) states are connected by local dimer fluctuations. The excitations created by breaking a dimer are two massive spinons, which propagate freely [15].

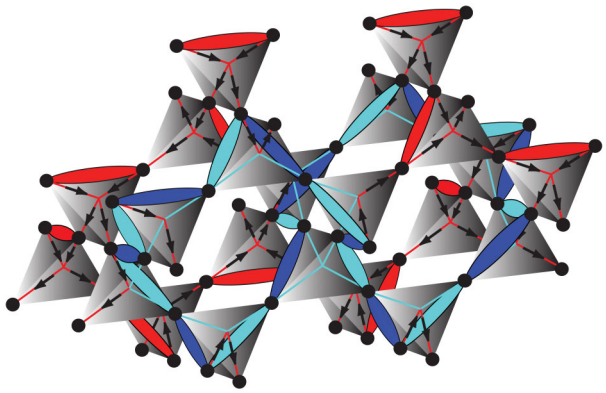

FIG. 3 (color). Dimer fluctuation process, shown as a loop of alternating light and dark blue dimers. This is a 22-bond loop (see text).

However, it is unrealistic to expect any physical system to be exactly at the Klein point. To understand which of its many properties may be preserved in a real material, it is essential to analyze the effect of perturbations. Because every site must be part of one dimer, the quantum mechanical fluctuations of the dimer liquid are local rearrangement processes on a closed path. Figure 2(d) illustrates the minimal possible dimer rearrangement on the pyrochlore lattice, and Fig. 3 shows more generally how all such processes may be described by loops, which represent the overlap of the two dimer coverings connected by the fluctuation. Here, we extend the loop-graph analysis of Ref. [15] to 3D to deduce the nature of the pyrochlore ground state close to the Klein point. A perturbation $\Delta H = \sum_{ij} \Delta J \mathbf{S}_i \cdot \mathbf{S}_j$ allows us to analyze exactly all the leading physically relevant terms in the pyrochlore Hamiltonian. Deviations from the Klein-point ratio, resulting from alterations to J_1 or J_2 in Eq. (3), are represented exactly by considering nearest-neighbor sites $\langle ij \rangle$, and deviations from $H = H_t$, particularly the J_3 terms in Eq. (4), are represented by using next-neighbor sites $\langle\langle ij \rangle\rangle$.

Loops, or dimer fluctuations, exist on all length scales, but as we show below the most important contributions are made by short loops, which describe local processes. The very shortest loops in the 3D (2D) pyrochlore lattice are 12- (8-)bond paths around a single hexagon [Fig. 2(d)] (vacant square [Fig. 2(c)]). Rearranging the 6 (4) dimers corresponds to flipping the sign of the arrow in the six-vertex representation, and we refer to local dimer configurations allowing these loops as "flippable plaquettes" [Figs. 2(c) and 2(d)]. These "Rokhsar-Kivelson" (RK) loops are zero-energy processes [15]. Nevertheless, dimer coverings with maximal numbers of flippable plaquettes also maximize longer contributing loops and, thus, form the basis for the new ground states in the presence of a perturbation. In 2D, two of the vertices are special in that all four edges of the square have an "in-out" arrow configuration [Fig. 2(a)], such that regular arrays of these two can

TABLE I. Lowest-order loops in the pyrochlore lattice [16].

Loop length	12	16	16	20	20	22	24	26
ΔH_{ab}	0	0	$\Delta J/128$	0	$-(\Delta J/512)$	$-(\Delta J/1024)$	$-(\Delta J/2048)$	$-(\Delta J/4096)$
Loop density	1	$\frac{1}{2}$	$\frac{1}{2}$	1	1	8	$\frac{1}{2}$	2

make every plaquette flippable [Fig. 2(c)]. The degeneracy of the submanifold of "maximally flippable" states is then $\mathcal{O}(1)$, and the ground states on both sides of the Klein point are valence-bond crystals, with a preferred static dimer order [15].

This result is a special property of the six-vertex model in a square geometry, and the situation in 3D is dramatically different. All six vertices are equivalent [Fig. 2(b)], and every tetrahedron has two edges destroying the flippability of the four associated hexagons (see Supplemental Material [16]), making it clear that not all hexagons in the 3D pyrochlore can be flippable. Our proof of spin-liquid nature around the Klein point is the demonstration (i) that the ground manifold has massive degeneracy and (ii) that this degeneracy is unbroken by any of the leading quantum fluctuations.

Flippable hexagons can be counted by considering the four interlocking kagome (111) planes of the pyrochlore lattice, highlighted in different colors in Fig. 1. The maximally flippable dimer coverings have bilayers of tetrahedra ensuring maximal flippability of the hexagons in two of the kagome planes, shown in blue and green in Fig. 1, interleaved with equivalent bilayers maximizing the other two planes (yellow and purple). The maximal number density of flippable hexagons is $1/3$ (see Supplemental Material [16]). Tetrahedra in the layer between the bilayers retain a twofold degree of freedom in singlet orientation (Fig. 1), equivalent to the relative arrow direction between bilayers. The degeneracy of the maximally flippable manifold is then $N_f = 9 \times 2^{L/3}$ [16], where the system volume is $N = L^3/4$ and L is the linear dimension.

To determine the ground manifold in the presence of physical perturbations, we evaluate the matrix elements of ΔH for each loop type; specifically, we compute $\Delta H_{ab} = \langle \psi_a | \Delta H | \psi_b \rangle$ for states $|\psi_a\rangle$ and $|\psi_b\rangle$ differing by one loop of dimers (Fig. 3). The importance of the maximally flippable configurations, anticipated above, is proven by considering all loops on the pyrochlore lattice involving two or three hexagons and generated by a single RK defect. The calculations are presented in Supplemental Material [16], and the results are summarized in Table I. Beyond the RK loop, the size of the matrix elements clearly falls exponentially with loop length, demonstrating the key role of the shortest loops. The ground manifold is, therefore, composed of all maximally flippable states containing precisely one RK defect, which may be on any one of the $N/3$ flippable hexagons, and hence, the dimension of this manifold of basis states $N_p = 3N \times 2^{L/3}$ is massive and exponential in L (Supplemental Material [16]).

To construct the ground-state wave function from this manifold, we require the loop density or number of each loop type per flippable hexagon. Whereas one type of 16-bond loop process contributes the most energy, the highest densities are found (Table I) for 22-bond loops, which correspond to flipping dimers around two hexagons sharing opposite edges of a single tetrahedron (Fig. 3). Unlike the 2D case, in 3D the lowest-order loops do interfere, and the deciding quantum fluctuations are the three shortest contributing loops in Table I (Supplemental Material [16]). By considering the most general linear combinations $|\psi\rangle = \sum_a c_a |\psi_a\rangle$ of states $|\psi_a\rangle$ based on the maximally flippable configurations with a single RK defect, we find that there are N_f distinct ground-state wave functions optimizing the loop (dimer fluctuation) contribution and that each of these is a superposition of $\mathcal{O}(N)$ basis wave-function pairs with equal amplitudes $|c_a|$ (Supplemental Material [16]). The sign of ΔJ causes differences not only in the phase structure of the variational wave functions (the signs of the coefficients $\{c_a\}$) [15,16] but also in their energies; we obtain $\Delta E = -(1/256)u^2 N \Delta J$ for $\Delta J > 0$ and $\Delta E = (1/128)v^2 N \Delta J$ for $\Delta J < 0$, where u, $v \simeq 1$ are normalization coefficients. Because 22-bond loops connect hexagons in neighboring bilayers, they can be used to illustrate a final, crucial property. There is no preferred direction for circumscribing a hexagon, and all such loops contribute the same energy for either maximally flippable dimer covering of each bilayer. By extension to any type of interbilayer loop (Supplemental Material [16]), there is no mechanism to lift the bilayer degeneracy, and hence, all N_p states in the ground manifold form the same type of minimum-energy state.

To summarize, our loop calculations verify that a highly degenerate ground manifold persists under physical perturbations away from the Klein point. Furthermore, all states in this manifold gain energy from mutual resonance. Linear combinations of these states span all dimensions and break no lattice symmetries. These are the qualitative energetic and spatial criteria for a spin liquid. However, a proof of quantum spin-liquid nature as a strict zero-temperature statement requires specific topological criteria. In the ground manifold of the non-Klein-point model, local loop processes reflect local gauge-type symmetries and their matrix elements determine the N_f variational ground states. These states are linked by $O(L^2)$ local processes, which correspond to system-scale, planar (dimension $d = 2$) loops, reflecting nonlocal "emergent" Z_2 symmetries associated with each bilayer (Supplemental Material [16]). In systems of finite size, this symmetry is broken, but the accompanying spectral gaps are exponentially small in L^2. The associated topological degeneracy in this and other models with $d \geq 1$ processes [18] is analogous to 2D quantum dimer models where the ground states are also equal-amplitude superpositions of dimer coverings. These models have nonlocal

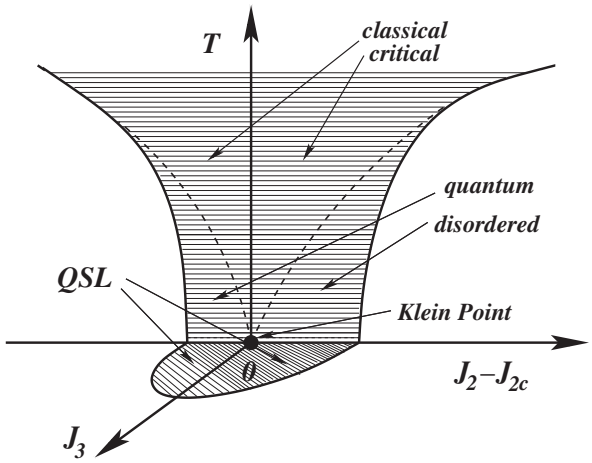

FIG. 4. Schematic phase diagram for the quantum spin liquid (QSL) phase of the $S = 1/2$ pyrochlore. $J_2 - J_{2c}$ and J_3 represent respectively the intra- and intertetrahedron perturbations away from the Klein point. Solid lines indicate phase transitions, and dashed lines indicate crossovers.

$d = 1$ symmetries associated with the parity of the even or odd number of dimers cut by 1D loops around the entire system and are understood as gapped quantum liquids with Z_2 topological order [8]. The extension of these topological concepts to dimer states in 2D systems of real $S = 1/2$ quantum spins has been demonstrated in recent detailed calculations [19,20]. Our analysis provides several key additional ingredients to this discussion (Supplemental Material [16]), proving rigorously from energetic and topological criteria that the pyrochlore spin model possesses zero-temperature quantum spin-liquid behavior in 3D over an extended region of the non-Klein-point parameter space, as represented in Fig. 4.

The basis states of this spin liquid are a subset of the Klein-point dimer coverings, and hence, are "divergence-free" in the six-vertex arrow representation (Fig. 2). It has been argued by analogy with continuum Gaussian electrostatics that spin-ice systems can be described by a U(1) gauge field theory (Supplemental Material [16]). However, for our microscopic model, where all states in the ground manifold are known exactly, as are all loop processes connecting them (Table I), we find that the local dimer rearrangements are more complex than those of a U(1) gauge theory alone. Independent of an approximate field-theory description, the variational ground states we have constructed at finite ΔJ are an exact quantum spin liquid, meaning that states in the ground manifold are no longer individual eigenstates of the non-Klein-point Hamiltonian and are connected by quantum fluctuations to all other states in the same topological sector.

In the schematic phase diagram of Fig. 4, the solid lines indicate phase transitions, which may be of first or second order; different types of ground state become increasingly competitive as the intratetrahedron singlet-triplet energy splittings increase, but in contrast to 2D a transition requires a finite separation from the Klein point. The dashed lines

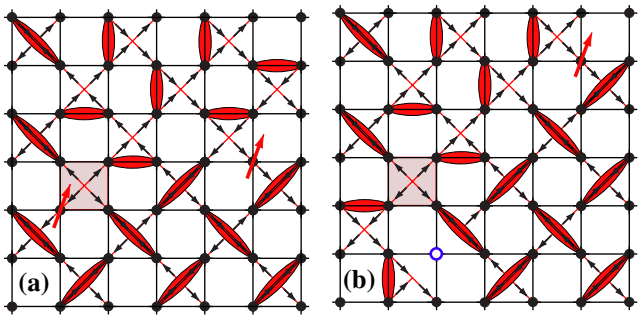

FIG. 5 (color online). Representation of (a) a dissociated spinon pair and (b) a spin-charge-separated spinon and hole.

indicate the energy scales for a thermally driven crossover from quantum to classical behavior, occurring when the temperature exceeds the splitting of the Klein-point manifold and the physics of the "Coulomb phase" of spinons is restored [15]. The absolute value of this splitting is remarkable. From the matrix elements in Table I, it is 2 orders of magnitude smaller even than the perturbation ΔJ, so that, even far from the Klein point, the entire manifold would be split on an energy scale well below 1 K for any real material. The practical criterion for spin-liquid nature is that no local probe can discern any type of order. At finite temperatures, any expectation value is a Gibbs average, a sum over exponentially many states with small (or vanishing) energy splittings, and thus will vanish for temperatures above (or below) the crossover (Supplemental Material [16]).

Armed with a microscopic model for a quantum spin-liquid state, we consider the nature of its excitations. High-dimensional fractionalization of both spin [15] and charge [21] degrees of freedom has been considered before in pyrochlore-based geometries. A spin excitation is the destruction of a dimer to create one defect tetrahedron (DT) and two free spins [Fig. 5(a)]. The finite energy cost for this process means these are massive spinons, with $m_s = 15J_2/16$ (Supplemental Material [16]). From the dimensional reduction [16] in our quantum spin liquid, the spinons are constrained to move on lines [22]. In the maximally flippable ground manifold (Fig. 1), the proliferation of local loops allows spinons to move easily from one line to another [15], and therefore, their motion is fully 3D. This ready availability of quantum fluctuations, exchanging spinon and dimer positions when H_t (3) is applied to individual tetrahedra [Fig. 5(a)], means that the spinons possess quantum dynamics and propagate at $T = 0$.

Charge degrees of freedom arise from a small concentration of dopants in the otherwise half-filled band. The energy penalty (a DT) is paid on introducing the hole, and the free spinon motion causes automatic spin-charge separation [Fig. 5(b)], leaving "holons" in the spin dimer background. Holon propagation occurs due to the kinetic term $-t\sum_{\langle ij\rangle,\sigma} c^{\dagger}_{i\sigma} c_{j\sigma}$ in H_{Hubb} (1). For such a lattice model in 3D, the statistics of spinons and holons can be computed from their hopping algebra [23], but this analysis requires a detailed treatment of projection operators describing

allowed states of the spin background and lies beyond the scope of the current Letter.

It is easy to show (Supplemental Material [16]) that holons experience a weak attraction to DTs. However, a direct binding would deny the holons the kinetic energy gain of propagating, albeit with a bandwidth highly renormalized by the spin background. Dynamical holons experiencing a mutually attractive interaction by lingering close to DTs would, by these simple considerations, have a weak tendency towards superconductivity. This superconducting state is driven not by the existence of valence-bond states [24] but by the special frustration near the Klein point.

We conclude by reviewing the possibilities for finding this spin-liquid state in a real pyrochlore material. The Klein-point value $t/U = 1/\sqrt{30}$ is well within the parameter range of typical correlated insulators. Unfortunately, despite the wealth of pyrochlore and spinel materials available, very few structurally regular $S = 1/2$ systems are known.

A fundamental property of the model (3) is that SU(2) spin symmetry is preserved, a requirement best satisfied by magnetic ions in the $3d$ series; to date the only candidates are the rare-earth vanadates $M_2V_2O_7$, which possess an additional t_{2g} orbital degeneracy and are ferromagnetic. For pyrochlores of $4d$ ions, the SU(2) character is removed by a significant spin-orbit coupling. Among $5d$ ions, pyrochlore iridates have received much recent attention [25] and possess an effective $J = 1/2$ degree of freedom, but it is not possible to obtain effective SU(2)-symmetric interactions in this geometry; these materials may also be too weakly interacting (borderline metallic) to approach the magnetic limit. However, we stress again one of our key results that energy scales for splitting of the degenerate manifold (Fig. 4) are very low, making spin-liquid behavior appear at any experimentally achievable temperatures even in systems with nontrivial perturbations from the Klein point. We suggest that pressure-dependent investigation of V^{4+} and Cu^{2+} materials may be the most promising avenue to find evidence for the spin-liquid state of the insulating spin-1/2 pyrochlore.

In summary, we have demonstrated rigorously that the half-filled one-band Hubbard model in the pyrochlore geometry hosts a 3D quantum spin liquid. This spin liquid emerges, over an extended parameter regime at zero temperature, from a highly degenerate manifold of valence-bond states. It possesses massive, deconfined spinon excitations and shows spin-charge separation on doping. It is a quantum mechanical state essentially different from those studied previously, including in the 2D pyrochlore [15]. This is one of the very few systems where unbroken degeneracies and exact deconfinement emerge in a realistic model with only short-range interactions. Finite-temperature evidence for such spin-liquid physics may be detectable in real pyrochlore materials.

We are indebted to C. Batista for his invaluable contributions. We thank R. Flint, Z.-C. Gu, Z. Hiroi, G. Ortiz, C. Rüegg, S. Sachdev, A. Seidel, and T. Senthil for helpful discussions and the Kavli Institute of Theoretical Physics for its hospitality. This work was supported by the NSF of China under Grant No. 11174365, by the National Basic Research Program of China under Grant No. 2012CB921704, and by the NSF under Grants No. CMMT 1106293 and No. PHY11-25915.

[1] P. W. Anderson, Mater. Res. Bull. **8**, 153 (1973).
[2] L. Balents, Nature (London) **464**, 199 (2010).
[3] R. Moessner and S. L. Sondhi, Phys. Rev. Lett. **86**, 1881 (2001); M. Hermele, T. Senthil, M. P. A. Fisher, P. A. Lee, N. Nagaosa, and X.-G. Wen, Phys. Rev. B **70**, 214437 (2004).
[4] P. Mendels and A. S. Wills, in *Introduction to Frustrated Magnetism*, edited by C. Lacroix, P. Mendels, and F. Mila (Springer, Heidelberg, 2011).
[5] K. Kanoda and R. Kato, Annu. Rev. Condens. Matter Phys. **2**, 167 (2011).
[6] B. Normand, Contemp. Phys. **50**, 533 (2009).
[7] U. Schollwöck, Rev. Mod. Phys. **77**, 259 (2005).
[8] E. Fradkin, *Field Theories of Condensed Matter Physics* (Cambridge University Press, Cambridge, England, 2013), 2nd ed.
[9] X.-G. Wen, *Quantum Field Theory of Many-Body Systems* (Oxford University, Oxford, 2004).
[10] T. Senthil, A. Vishwanath, L. Balents, S. Sachdev, and M. P. A. Fisher, Science **303**, 1490 (2004).
[11] R. J. Baxter, *Exactly Solved Models in Statistical Mechanics* (Academic, London, 1982).
[12] D. J. Klein, J. Phys. A **15**, 661 (1982).
[13] J. T. Chayes, L. Chayes, and S. A. Kivelson, Commun. Math. Phys. **123**, 53 (1989).
[14] A. Seidel, Phys. Rev. B **80**, 165131 (2009).
[15] Z. Nussinov, C. D. Batista, B. Normand, and S. A. Trugman, Phys. Rev. B **75**, 094411 (2007); **88**, 219903(E) (2013).
[16] See Supplemental Material at http://link.aps.org/supplemental/10.1103/PhysRevLett.112.207202 for details.
[17] L. Pauling, *The Nature of the Chemical Bond* (Cornell University, Ithaca, 1939).
[18] Z. Nussinov and G. Ortiz, Proc. Natl. Acad. Sci. U.S.A. **106**, 16944 (2009).
[19] D. Poilblanc, N. Schuch, D. Pérez-García, and J. I. Cirac, Phys. Rev. B **86**, 014404 (2012).
[20] J. Wildeboer and A. Seidel, Phys. Rev. Lett. **109**, 147208 (2012).
[21] P. Fulde, K. Penc, and N. Shannon, Ann. Phys. (Berlin) **11**, 892 (2002).
[22] C. D. Batista and S. A. Trugman, Phys. Rev. Lett. **93**, 217202 (2004).
[23] M. Levin and X.-G. Wen, Phys. Rev. B **67**, 245316 (2003).
[24] P. W. Anderson, Science **235**, 1196 (1987).
[25] W. Witczak-Krempa, G. Chen, Y.-B. Kim, and L. Balents, Annu. Rev. Condens. Matter Phys. **5**, 57 (2014).